Polarity conversion of GaN nanowires grown by plasma-assisted molecular beam epitaxy

Alexandre Concordel, Gwenolé Jacopin, Bruno Gayral, Núria Garro, Ana Cros, Jean-Luc Rouviere, Bruno Daudin

Polarity conversion of GaN nanowires grown by plasma-assisted molecular beam epitaxy

Alexandre Concordel[1], Gwénolé Jacopin[2], Bruno Gayral[1], Núria Garro[3], Ana Cros[3], Jean-Luc Rouvière[4] and Bruno Daudin[1]*

[1]*Université Grenoble Alpes, CEA, INAC, F-38000 Grenoble, France*

[2] *Institut Néel, Université Grenoble Alpes, CNRS, Grenoble INP, 38000 Grenoble, France.*

[3]*Institute of Materials Science (ICMUV), Universidad de Valencia, P.O. Box 22085, Valencia, Spain*

[4] *CEA, INAC-MEM, LEMMA, F-38000 Grenoble, France*

Abstract

It is demonstrated that the N-polarity of GaN nanowires (NWs) spontaneously nucleated on Si (111) by molecular beam epitaxy can be reversed by intercalation of an Al- or Ga-oxynitride thin layer. The polarity change has been assessed by a combination of chemical etching, Kelvin probe force microscopy, cathodo- and photoluminescence spectroscopy and transmission electron microscopy experiments. Cathodoluminescence of the Ga-polar NW section exhibits a higher intensity in the band edge region, consistent with a reduced incorporation of chemical impurities. The polarity reversal method we propose opens the path to the integration of optimized metal-polar NW devices on any kind of substrates.

*corresponding author: bruno.daudin@cea.fr

The current revolution in solid state lightning is relying to a large extent on light-emitting diodes (LEDs) based on InGaN/GaN heterostructures. In spite of the relatively high density of extended defects due to the lack of lattice-adapted substrate, the external quantum efficiency (EQE) of these LEDs is remarkably high for blue emission, over 80%, when grown on sapphire [1] as well as on Si substrates [2, 3]. However, EQE drops continuously for larger wavelength emission, i.e. for increasing InN molar fraction in InGaN QWs, a feature commonly known as the green gap issue. Such a decrease in EQE originates from three complementary effects: the cumulative amount of defects for increasing lattice mismatch between the InGaN QW and the GaN barrier, alloy composition fluctuations, and the influence of quantum confined Stark effect (QCSE), that intensifies for large InN molar fraction [4, 5]. In such a context, InGaN/GaN nanowire (NW) heterostructures appear as a potential solution to overcome, at least partially, the limitations of conventional QW-based heterostructures. Indeed, their small diameter and high length/diameter aspect ratio are favorable to the strain relaxation of the heterostructures resulting in a decrease of the QCSE and an increase in carrier recombination efficiency. This especially holds for NWs grown by plasma-assisted molecular beam epitaxy (PA-MBE), which exhibit a diameter in the 50-100 nm range and are mostly free of extended defects [6-9].

Self-organized, catalyst-free GaN NWs have been grown on a variety of substrates, namely Si(111) and Si(100) [10], sapphire [6], SiO_2 [11], SiC (with an AlN buffer) [12], diamond [13], graphite [14], titanium and tantalum foils [15-17]. Whatever the substrate, it has been found that these NWs mostly exhibited N-polarity, even if a careful chemical pretreatement may in some cases lead to a significant fraction of metal-polar NWs [17 bis].However, N-polar NWs are intrinsically improper to the realization of efficient devices because of the easy incorporation of impurities on the N-polar surface [18], which motivates the efforts to develop a strategy to convert their polarity from N-polar to metal-polar.

In the field of thin layer growth, several strategies have been considered in the past to reach this target. On the one hand, GaN layers polarity conversion from N-polar to metal-polar has been achieved by exposure to Mg [19], which has been assigned to the formation of an Mg_xN_y interlayer, likely consisting of Mg_3N_2 [20-22].

On the other hand, polarity conversion has been demonstrated by depositing an Al metallic layer on top of one N-polar GaN layer. The overgrown GaN layer deposited on top of this Al-saturated surface was shown to exhibit a Ga-polarity [23]. A similar result has been

obtained by M. Adachi and coworkers on AlN layers grown by liquid phase epitaxy. Interestingly, in this last case the role of oxygen partial pressure during growth was pointed out and the polarity inversion mechanism has been assigned to the formation of an octahedrally coordinated Al layer resulting in the reset of the nitridated sapphire surface [24]. The combined effect of oxidation and AlN layer has been emphasized by Wong et al [25] who have shown that polarity of a N-polar GaN layer could be inverted by deposition of a thin AlN layer on top followed by atmosphere exposure and further deposition of a thin AlN layer. Importantly, the second AlN layer was found to be necessary to ensure full polarity conversion, while direct GaN growth on oxidized AlN layer only resulted in partial polarity conversion. Recently Mohn and coworkers have further studied the mechanisms fixing the polarity of AlN grown on sapphire at the atomic scale and concluded that the formation of an $Al_xN_yO_z$ layer was responsible for the conversion of the initial N-polar surface into an Al-polar one [26]. Inspired by these previous works, it is the goal of the present study to address the issue of polarity conversion of spontaneously nucleated GaN nanowires from N-polar to Ga-polar.

GaN NWs were grown by plasma-assisted molecular beam epitaxy (PA-MBE) on Si (111) substrates. Prior to the growth, the Si (111) substrate was deoxidized in HF at 10% followed by an outgassing stage in the growth chamber till appearance of the 7x7 surface reconstruction characteristic of a clean, oxide-free surface. All samples were grown in N-rich conditions at a growth temperature of 830°C measured using a thermocouple facing the rear face of the sample holder. Sample #1 consisted of untreated GaN NWs, about 2 μm long, shown in figure 1. Their polarity was assessed by KOH etching: all NWs exhibit a facetted top surface after etching consistent with their N-polar character [27].

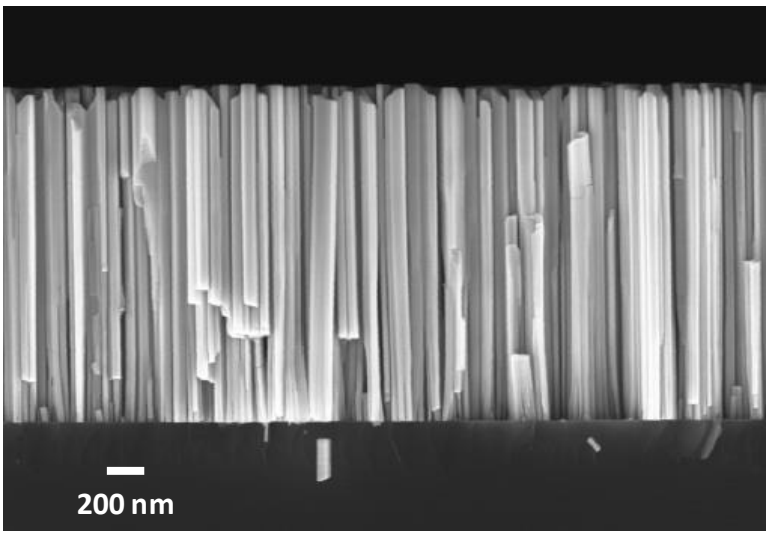

Figure 1: Scanning electron microscopy (SEM) view of GaN NWs (Sample #1).

Sample #2 was grown in two steps: at the end of the first step of the growth, corresponding to GaN NWs about 1 micrometer long, the sample was covered with an AlN cap grown in nearly stoichiometric conditions and taken out from the MBE machine for oxidation. Based on Al cell flux calibration using RHEED oscillations, the nominal thickness of the AlN layer was about 5 monolayers (MLs). Oxidation was performed during 10 s using a Nextral ICP machine. The O flux was 60 sccm, for a power of 30 W and a pressure of 0.1 torr. Next, the sample was introduced again in the MBE for completion of the growth, namely the deposition of a nominally 5 MLs thick AlN section, followed by GaN deposition in conditions identical to those used for growing the first section till reaching a total length of about 2 micrometers. KOH etching at room temperature under day light has put in evidence that a significant number of NWs were insensitive to etching, as a first clue of the effectiveness of the intermediate layer to flip the N-polarity. For further comparison, sample #3 consisted of a non oxidized GaN/AlN/GaN NW heterostructure, the thickness of AlN (about 10 MLs) being equal to the total amount of AlN in sample #2. Finally, sample #4 consisted of GaN NWs, with a growth interruption after 1 μm followed by air oxidation during one night and further growth of a 1 μm upper section.

The polarity of samples #1 and #2 was further studied by Kelvin probe force microscopy (KPFM) following the same procedure as that described in ref. [28]. Figure 2a and b shows the AFM and the corresponding surface potential scan, respectively, of sample #1. As put in evidence in figure 2c, the mean potential corresponds to N-polarity and only one NW in the picture is exhibiting a surface potential value consistent with Ga polarity. It is concluded that the amount of Ga-polar NWs in this sample does not exceed a few percent, in agreement with previous work [29]. By contrast, as shown in figure 2d, e and f, results concerning sample #2 demonstrate that the surface potential value is close to that expected for Ga-polar material for the whole sample, suggesting that NWs polarity has been flipped from N to Ga. The ~100 mV offset of the surface potential value with respect to the value expected for Ga-polar NWs is tentatively assigned to the formation of the interlayer.

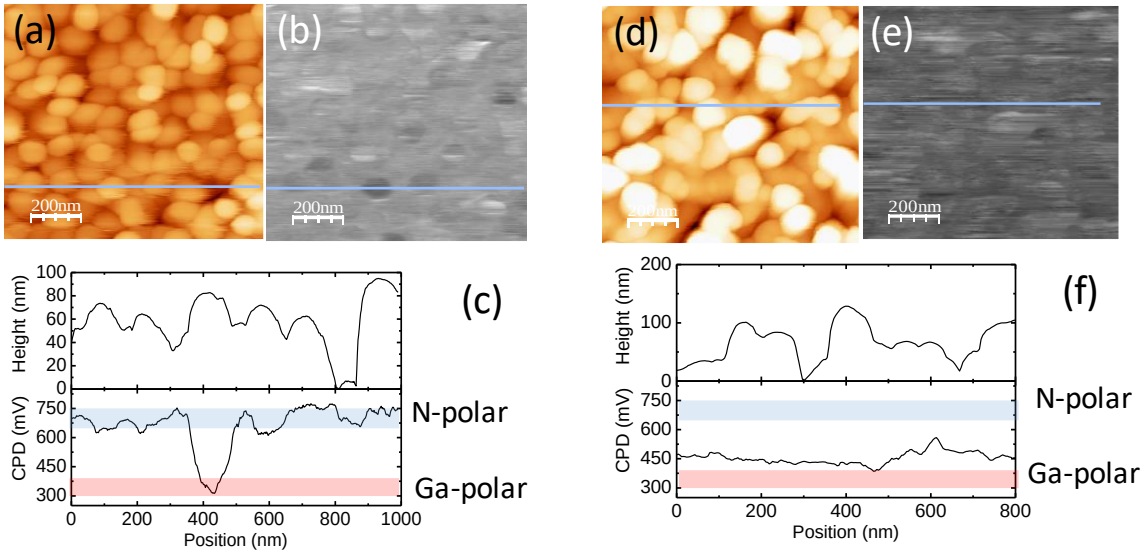

Figure 2: a) AFM image and b) surface potential scans of sample #1 c) topography and surface potential profiles, respectively taken along the blue line shown in a) and b). d) AFM image and e) surface potential scans of sample #2. f) Topography and surface potential profiles, respectively taken along the blue line shown in d) and e). The blue and pink bands in c) and f) mark the Contact Potential Difference (CPD) value measured in the N and Ga-polar faces of a reference sample grown by HVPE [25]. The scale of both surface potential maps spans from 0 to 1.2 V.

Optical properties of the four samples under investigation were studied by photoluminescence (PL) spectroscopy. The data are shown in figure 3a. The PL spectrum of sample #1 is dominated by band edge emission around 3.47 eV, with a faint shoulder at 3.45 eV. It has to be reminded that the emission at 3.45 eV has been assigned to the presence of inversion domain boundaries (IDBs) in NWs [30]. Then, this shoulder is assigned to the scarce NWs exhibiting either Ga-polarity or mixed polarity, consistent with KPFM data. By contrast, the PL spectrum of sample #2 exhibits a clear signature at 3.45 eV, indicative of the presence of IDBs. In absence of oxidation step, no 3.45 eV PL component is seen in the PL spectrum of sample #3 containing an inserted AlN layer of equivalent thickness, pointing out the determinant role of oxygen in the formation of the intermediate layer triggering the polarity flipping. Finally, the PL spectrum of sample #4 also exhibits a component at 3.45 eV suggesting that GaN oxidation itself without the presence of an AlN layer is sufficient to trigger polarity flipping.

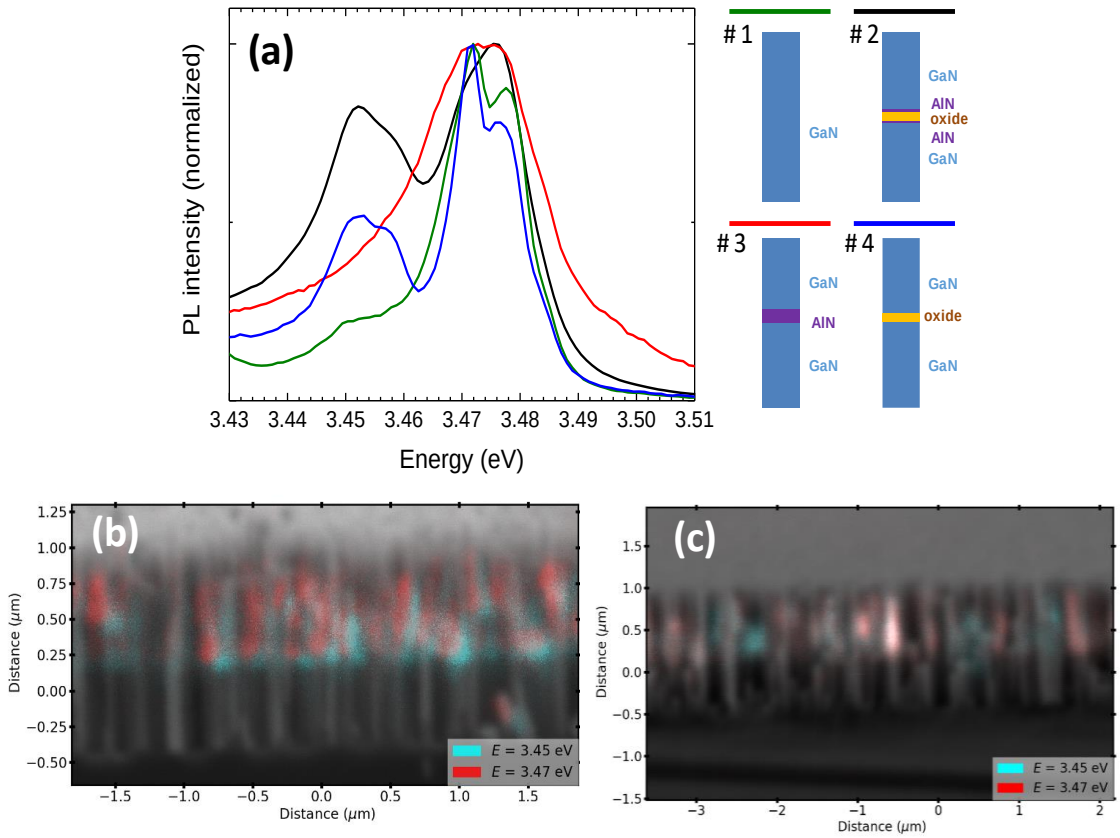

Figure 3: (a) Photoluminescence spectra of four samples grown according to the corresponding schemes. Note the presence of a 3.45 eV component in sample#2 with the double oxidized AlN interlayer (black) and in sample #4 consisting of pure GaN NWs with a growth interruption for air oxidation (blue). (b) 3.45 and 3.47 eV cathodoluminescence mapping of sample #2. (c) the same for sample #4.

To further analyse the effect of the oxidized AlN interlayer at nanometric scale, we performed cathodoluminescence (CL) spectroscopy on an ensemble of NWs from a cleaved piece of sample #2 and sample #4. To achieve a good spatial resolution (≈50 nm), a 3kV acceleration voltage has been used. CL has been collected thanks to a parabolic mirror and analysed thanks to fast PMT detector coupled to Horiba IhR550 spectrometer with a 600 grooves/mm diffraction grating.

The results are shown in figure 3b and 3c where the CL maps for 3.45 and 3.47 eV emission energies have been superimposed to the SEM images of the NWs. For sample #2, the 3.45 eV emission is mostly present in the region associated with the presence of the oxidized AlN interlayer and is also observed in the upper part of a significant fraction of the

NWs. This strongly supports the presence of IDBs associated with the oxidized AlN interlayer and extending in the NW upper part. Interestingly, the 3.47 eV emission corresponding to band edge is more intense in the upper part of the NWs, supporting the hypothesis of increased band edge emission due to reduced chemical impurity incorporation in the Ga-polar NWs portion, with respect to their N-polar section counterpart. Similar results are shown in figure 3b for sample #4, namely the coexistence of both 3.45 and 3.47 eV contributions in the upper part of the NWs. However, the wide extension of 3.45 eV map suggests that, contrary to the case of sample #2 most IDBs in this case are threading from the oxidized layer to the top surface.

To unambiguously assess the formation of IDBs associated with the oxidized interlayer convergent beam electron diffraction (CBED) and high resolution scanning transmission electron microscopy (HR-STEM) have been performed on a Thermo Fisher Scientific TITAN Ultimate double Cs-corrected machine. A convergent angle of about 20mrad was used for HR-STEM. To obtain sharper CBED pattern the C3-condensor was switched off and the beam size broadened to about 2 nm by decreasing the convergence angle to 2.4 mrad. Energy Dispersive X-ray (EDX) spectroscopy have been performed on a Thermo Fisher Scientific TITAN Themis equipped with 4 EDX detectors and a probe Cs-aberration corrector. Samples for cross-sections TEM observations have been thinned by tripode polishing. The results are displayed in figure 4a and 4b where the oxidized AlN interlayer is clearly shown. The formation of AlN/GaN NW heterostructures has been extensively studied, putting in evidence the formation of chemically abrupt interfaces [31-33]. This is consistent with the high resolution TEM image shown in figure 4e, where the oxidized AlN layer is shown to exhibit sharp interface with GaN above and below it. Such a feature is further confirmed by EDX Al profile shown in figure 5c where Al peak is associated with a sharp dip in the Ga EDX spectrum. The O EDX profile also reveals that O is peaked at a position superimposed to the AlN layer, combined with a marked diffusion far away from both sides of the oxidized layer. In the Al and Ga EDX profiles shown in figure 5b, the apparent Ga/Al intermixing visible in the lower part of the AlN layer is indeed related to the peripheral curvature of the AlN layer clearly visible in figure 4b and 5a, which results in a superposition of GaN and AlN. As shown in figure 4c and d, convergent beam electron diffraction (CBED) experiments performed above and below the interfacial region have put in evidence a 180° rotation, unambiguously assigned to a switch from N-polar to Ga-polar crystallographic orientation along the growth axis. Moreover, the structure with whitish contrast above the

oxidized AlN interlayer (figure 4a and 4b) was found to consist of a mixture of Ga and N polarity material.

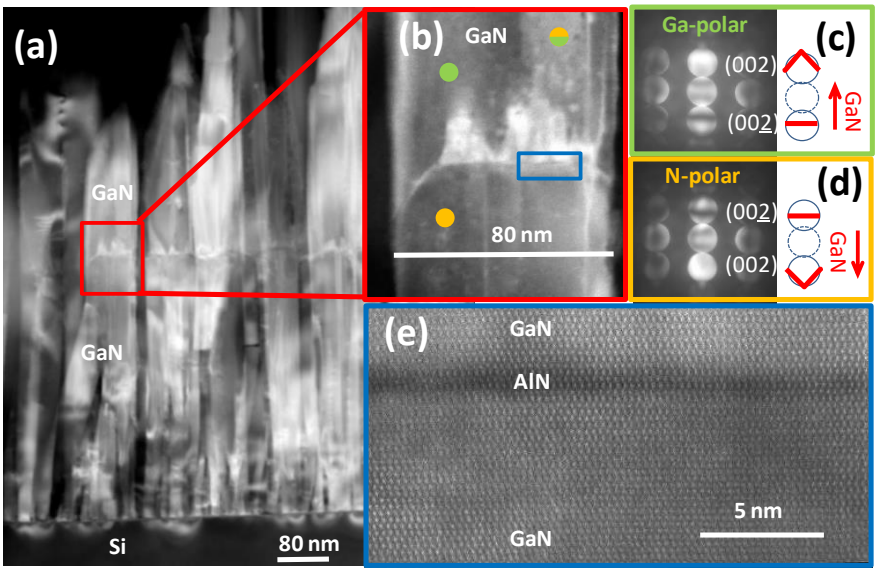

Figure 4: (a) Cross-section TEM observation of sample #2. (b) STEM image zooming on the oxidized AlN interlayer region. The colored dots indicate the spots chosen for CBED experiments. Mixed polarity was observed in the upper right corner. (c) CBED diagram indicative of Ga-polarity in the upper part of the NW, 180°-reverted with respect to (d) the lower part exhibiting N-polarity. (e) High resolution STEM image of the oxidized AlN layer.

Interestingly, the mixed polarity character of GaN just above the oxidized AlN layer is consistent with CL data reported in figure 3, i.e. the evidence for a high density of IDBs in the interface region, which is assessed by the 3.45 eV optical emission. These features actually demonstrate that the polarity flipping induced by the oxidation stage is not complete. Furthermore, it suggests that the growth rate of Ga-polar domains is larger than the growth rate of N-polar ones, eventually leading to the prevalence of Ga-polarity to the expense of N-polar domains. The polarity dependence of GaN growth rate for identical growth parameters has been examined by Koukitu et al [34]. These authors have established that at high temperature the growth rate of Ga-polar GaN is larger than the growth rate of its N-polar counterpart and vice versa at low temperature. In the high temperature regime of NW growth, it is therefore expected that the growth rate of Ga-polar domains will be higher, consistent with the progressive vanishing of N-polar domains deduced from CL reported in figure 3 and from TEM results.

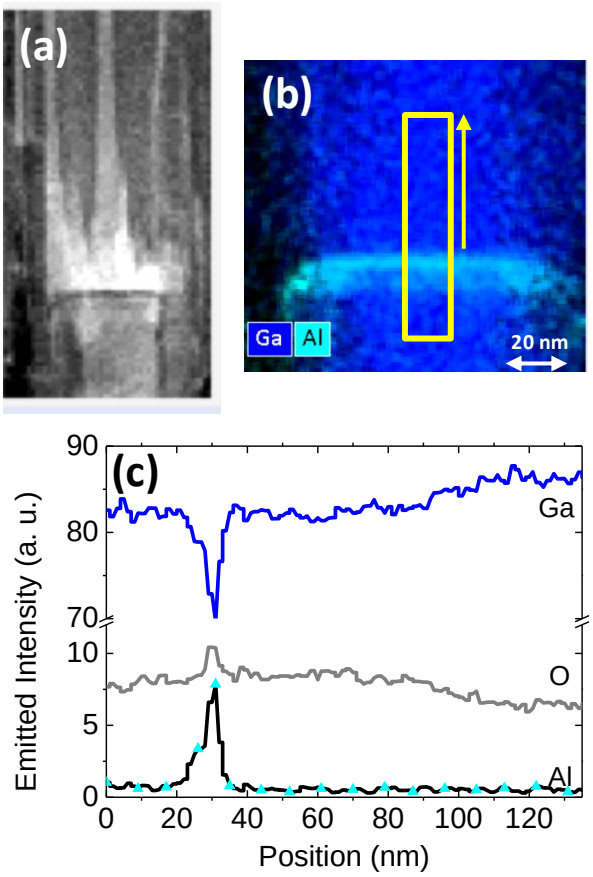

Figure 5: (a) HAADF image of the interlayer and GaN section besides, (b) Al and Ga EDX mapping zoomed around the interlayer area showed in (a). (c) EDX profile along the growth axis (yellow framed area) showing correlated Al and O peaks and anti-correlated Ga peak.

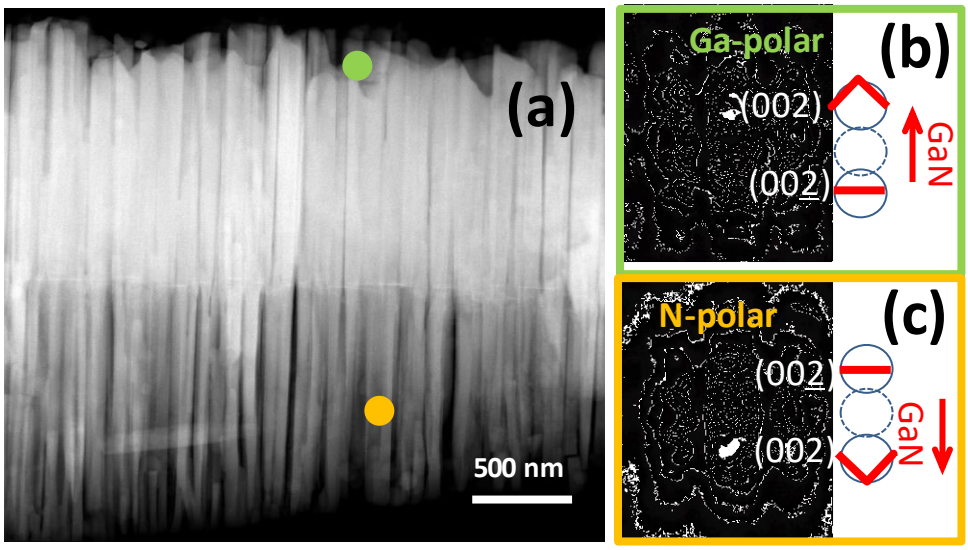

Figure 6: sample #4. (a) GaN NWs with the layer resulting from an oxidation step in air. Colored dots correspond to: (b), (c) CBED diffraction patterns showing the polarity flipping from N-polar to Ga-polar associated with the oxidation step.

Cross-section TEM observation of sample #4 is shown in figure 6. Similar to the case of sample #2, CBED diagrams taken below and above the oxidized GaN layer demonstrate a polarity flipping, induced by the single oxidation step of GaN NW top surface. Indeed, following the demonstration of the mechanism leading to Al-polar character of AlN layers grown on sapphire [26], Stolyarchuk and coworkers have recently demonstrated that N-polarity of AlN layers could be inverted by intentional exposure to O plasma [35] leading to the formation of a self-limited aluminum-oxynitride structure. The present results demonstrate that a similar mechanism may allow the polarity conversion of N-polar GaN NWs by using an oxidized AlN interlayer. Furthermore, the formation of IDBs in GaN NWs having experienced an air oxidation step during the growth process combined with TEM results in figure 6 put in evidence that a Ga-oxynitride layer has a similar effect, emphasizing the role of interfacial oxygen incorporation as the key-factor to trigger polarity conversion.

In summary, it has been established that the deposition of an AlN interlayer followed by plasma oxidation leads to the polarity flipping of GaN NWs spontaneously nucleated on Si (111). The polarity conversion has been assessed to the formation of an Al-O-N intermediate layer, likely analogous to the Al-oxynitride layer reported to account for AlN polarity conversion following O plasma exposure. Additionally, similar results on GaN NWs deprived of AlN interlayers demonstrate that the formation of a Ga-O-N intermediate layer tentatively consisting of a Ga-oxynitride is responsible for polarity flipping. As a whole, the conversion of GaN NWs from N-polar to Ga-polar opens the path for the realization of efficient axial, metal-polar NW light emitting diodes on a variety of substrates including metallic and soft ones.

Acknowledgements: We acknowledge Nicolas Mollard for the preparation of TEM samples and Dr. Walf Chikhaoui for O plasma experiments. We thank Dr. C. Bougerol and Dr. P. Vennégues for fruitful discussions. A. C. and N. G. acknowledge financial support from project ENE2016-79282-C5-3-R from the Spanish MICINN and PROMETEO/2018/123 from Generalitat Valenciana.

References

[1] Yukio Narukawa, Masatsugu Ichikawa, Daisuke Sanga, Masahiko Sano and Takashi Mukai, J. Phys. D: Appl. Phys. **43,** 354002 (2010)

[2] Shigeya Kimura, Hisashi Yoshida, Toshihide Ito, Aoi Okada, Kenjiro Uesugi, Shinya Nunoue, Proc. SPIE 9748, Gallium Nitride Materials and Devices XI, 97481U (26 February 2016); doi: 10.1117/12.2211880

[3]L.Y. Kuritzky, A.C. Espenlaub, B.P. Yonkee, C.D. Pynn, S. P. Denbaars, S. Nakamura, C. Weisbuch and J. S. Speck, Optics Express, **25**, 30696 (2017)

[4] Matthias Auf der Maur, Alessandro Pecchia, Gabriele Penazzi, Walter Rodrigues, and Aldo Di Carlo, Phys. Rev. Lett. **116**, 027401 (2016)

[5] Chi-Kang Li, Marco Piccardo, Li-Shuo Lu, Svitlana Mayboroda, Lucio Martinelli, Jacques Peretti, James S. Speck, Claude Weisbuch, Marcel Filoche, and Yuh-Renn Wu, Phys. Rev. B **95**, 144206 (2017)

[6] Masaki Yoshizawa, Akihiko Kikuchi, Masashi Mori, Nobuhiko Fujita and Katsumi Kishino, Jpn. J. Appl. Phys. **36**, L459 (1997).

[7] M. Yoshizawa, A. Kikuchi, N. Fujita, K. Kushi, H. Sasamoto, and K. Kishino, J. Cryst. Growth **189/190**, 138 (1998)

[8] M.A.Sanchez-Garcia, E. Calleja, E.Monroy, F.J. Sanchez, F. Calle, E. Munoz, R.Beresford, J. Cryst. Growth **183**, 23 (1998).

[9] E. Calleja, M.A. Sanchez-Garcia, F.J. Sanchez, F. Calle, F.B. Naranjo,E. Munoz, S.I. Molina, A.M. Sanchez, F.J. Pacheco, R. Garcia J. Cryst. Growth **201/202**, 296 (1999)

[10] E. Calleja, J. Ristic, S. Fernández-Garrido, L. Cerutti, M. A. Sánchez-García, J. Grandal, A. Trampert, U. Jahn, G. Sánchez, A. Griol, and B. Sánchez, Physica status solidi (b), **244**, 2816 (2007)

[11] Toma Stoica, Eli Sutter, Ralph J. Meijers, Ratan K. Debnath, Raffaella Calarco, Hans Lüth, and Detlev Grützmacher, Small, **4**, 751 (2008)

[12] Sergio Fernández-Garrido, Xiang Kong, Tobias Gotschke, Raffaella Calarco, Lutz Geelhaar, Achim Trampert, and Oliver Brandt, Nano Lett. **12**, 6119 (2012)

[13] Fabian Schuster, Florian Furtmayr, Reza Zamani, Cesar Magén, Joan R. Morante, Jordi Arbiol, Jose A. Garrido, and Martin Stutzmann, Nano Lett.**12**, 2199 (2012)

[14] Shinta Nakagawa, Takuya Tabata, Yoshio Honda, Masahito Yamaguchi, and Hiroshi Amano, Jpn. J. Appl. Phys. **52,** 08JE07 (2013)

[15] G. Calabrese, P. Corfdir, G. Gao, C. Pfüller, A. Trampert, O. Brandt, L. Geelhaar, and S. Fernández-Garrido, Appl. Phys. Lett. **108**, 202101 (2016).

[16] B.J. May, A.T.M.G. Sarwar, and R.C. Myers, Appl. Phys. Lett. **108**, 141103 (2016).

[17] G. Calabrese, S.V. Pettersen, C. Pfüller, M. Ramsteiner, J. Grepstad, O. Brandt, L. Geelhaar, and S. Fernández-Garrido, Nanotechnology **28**, 425602 (2017).

[17bis] Martin Hetzl, Max Kraut, Theresa Hoffmann, and Martin Stutzmann, Nano Letters **17**, 3582 (2017)

[18] F. Feix, T. Flissikowski, K.K. Sabelfeld, V.M. Kaganer, M. Wölz, L. Geelhaar, H.T. Grahn, and O. Brandt, Ga-Polar (In,Ga)N/GaN, Phys. Rev. Appl. **8**, 14032 (2017)

[19] M. H. Wong, F. Wu, T. E. Mates, J. S. Speck, and U. K. Mishra, J. Appl. Phys. **104**, 093710 (2008)

[20] V. Ramachandran, R. M. Feenstra, W. L. Sarney, L. Salamanca-Riba, J. E. Northrup, L. T. Romano and D. W. Greve, Appl. Phys. Lett. **75**, 808 (1999)

[21] N. Grandjean, A. Dussaigne, S. Pezzagna, and P. Vennéguès, J. Cryst. Growth **251**, 460 (2003)

[22] J. Northrup, Appl. Phys. Lett. **82**, 2278 (2003)

[23] K. Xu, N. Yano, A. W. Jia, A. Yoshikawa and K. Takahashi, phys. stat. sol. (b) **228**, 523 (2001)

[24] Masayoshi Adachi, Mari Takasugi, Masashi Sugiyama, Junji Iida, Akikazu Tanaka, and Hiroyuki Fukuyama, Phys. Status Solidi B **252**, 743 (2015)

[25] Man Hoi Wong, Feng Wu, James S. Speck, and Umesh K. Mishra1 J. Appl. Phys. **108**, 123710 (2010)

[26] S. Mohn, N. Stolyarchuk, T. Markurt, R. Kirste, M.P. Hoffmann, R. Collazo, A. Courville, R. Di Felice, Z. Sitar, Ph. Vennéguès, and M. Albrecht, Phys. Rev. Appl. **5**, 054004 (2016).

[27] Karine Hestroffer, Cédric Leclere, Catherine Bougerol, Hubert Renevier and Bruno Daudin, Phys. Rev. B **84**, 245302 (2011)

[28] A. Minj, A. Cros, N. Garro, J. Colchero, T. Auzelle, and B. Daudin, Nano Lett. **15**, 6770 (2015)

[29] Thomas Auzelle, Benedikt Haas, Albert Minj, Catherine Bougerol, Jean-Luc Rouvière, Ana Cros, Jaime Colchero, and Bruno Daudin, J. Appl. Phys. **117**, 245303 (2015)

[30]Thomas Auzelle, Benedikt Haas, Martien Den Hertog, Jean-Luc Rouvière, Bruno Daudin, and Bruno Gayral, Appl. Phys. Lett. **107**, 051904 (2015)

[31] J. Renard, R. Songmuang, G. Tourbot, C. Bougerol, B. Daudin and B. Gayral, Phys. Rev. B **80**, 121305R (2009)

[32] P. Hille, J. Müßener, P. Becker, M. de la Mata, N. Rosemann, C. Magén, J. Arbiol, J. Teubert, S. Chatterjee, J. Schörmann and M. Eickhoff, Appl. Phys. Lett. **104**, 102104 (2014)

[33] Jonas Lähnemann, Akhil Ajay, Martien I. Den Hertog, and Eva Monroy, Nano Lett., **17** (11), 6954 (2017)

[34] Akinori Koukitu, Miho Mayumi, Yoshinao Kumagai, J. Cryst. Growth **246** 230 (2002)

[35] N. Stolyarchuk, T. Markurt, A. Courville, K. March, J. Zúñiga-Pérez, P. Vennéguès and M. Albrecht, Sc. Reports **8**, 14111 (2018)